Characteristics of Speed–Acceleration Phase Diagram of Migrating Cells

Yikai Ma(马一凯) and Wei Chen(陈唯)*

State Key Laboratory of Surface Physics and Department of Physics, Fudan University, Shanghai 200438, China

(Received 19 September 2023; accepted manuscript online 10 November 2023)

Cell movement behavior is one of the most interesting biological problems in physics, biology, and medicine. We experimentally investigate the characteristics of random cell motion during migration. Observing cell motion trajectories under a microscope, we employ a nonlinear dynamics method to construct a speed–acceleration phase diagram. Our analysis reveals the presence of a fixed point in this phase diagram, which suggests that migrating cells possess a stable state. Cells that deviate from this stable state display a tendency to return to it, following the streamline trends of an attractor structure in the phase diagram. We derive a set of characteristic values describing cell motion, encompassing inherent speed, inherent acceleration, characteristic time for speed change, and characteristic time for acceleration change. We develop a differential equation model based on experimental data and conduct numerical calculations. The computational results align with the findings obtained from experiments. Our research suggests that the asymmetrical characteristics observed in cell motion near an inherent speed primarily arise from properties of inherent acceleration of cells.

DOI: 10.1088/0256-307X/40/12/128701

Cell migration is a crucial issue in biology, medicine, and physics. Research of cell motion can provide valuable insights into migration mechanisms of cells in different environments, elucidating their roles in important processes such as development, tissue formation, and immune response.[1–3] Physicists have developed multiple models, such as the generalized Langevin equation and fractal differential equations, to comprehend the characteristics of cell migration based on the theory of random walks.[4–8] The motion of cells under diverse conditions has been extensively investigated.[9–11] However, our understanding of the complex behavior of cell movement remains insufficient. Due to the anomalous diffusion nature of cells, their behavior significantly deviates from classical random walk theory[9,12,13] and there is no consensus on the characteristic values that describe their behavior. In this work, we experimentally study the characteristics of migration of *dictyostelium discoideum* (Dicty) cells. We employ nonlinear dynamics, a valuable tool for understanding complex systems and previously utilized extensively to investigate cellular behavior,[14,15] to construct a speed–acceleration phase diagram of cell movement utilizing experimental data. Nonlinear dynamics research has mainly been used to study the internal molecular mechanisms of cell movement[16] or pulse waves of cAMP propagation.[17,18] In 2019, a study by Brückner *et al.*[15] showed that the nonlinear dynamics of cell movement in confinement can be characterized as a limit cycle or excitable bistable dynamics. In this work, we investigate the nonlinear dynamical characteristics of cells during free locomotion. Through quantitative analysis of the phase diagram, we find that the dynamic model of Dicty cell movement without confinement conforms to the attractor form within the framework of nonlinear dynamics. This analysis investigates the fundamental properties of cellular migration, and offers a research framework for studying the dynamics of migrating cells. The framework has broad applicability in examining the characteristics of cell migration behavior under diverse conditions.

In this work, Dicty cells were used as the research object. The methods for cell preparation and experimental observation were based on Chen *et al.*[19] First, we prepared agar by dissolving 20 g of agarose (Sigma, USA) in 1 L of distilled water. The pH of the agar solution was adjusted to 6.0–6.4, followed by autoclaving at high pressure (0.142 MPa) and temperature (126 ℃) for 20 min. Subsequently, the hot medium was carefully poured into sterilized culture dishes in a sterile environment, with each dish being filled approximately one-third full with the solid medium. Then, we starved the cells at 5 ℃ for 2 h to induce the migration mode. Subsequently, the starved Dicty cells were planted on a non-nutrient agar (98% w/v) surface with a density of 60 cells/mm^2 at room temperature. Motion images of the cells were continuously captured for 30 h using an Olympus CX23 microscope (4× objective) and a Canon EOS 100D digital camera. The spatial resolution of the camera was 5184×3456, with a time interval (Δt) of 30 s. We employed a self-made IDL program to identify and track the cell trajectories $r(t)$.

Based on the cellular movement trajectories $r(t)$, as shown in Fig. 1(a), we can calculate the cell speed $v = |\Delta r/\Delta t|$ and acceleration $a = \Delta v/\Delta t$ for each moment. The probability distribution of cell speed $P(v)$ is plotted in Fig. 1(b). From the semi-log plot, as shown in Fig. 1(b),

*Corresponding author. Email: phchenwei@fudan.edu.cn
© 2023 Chinese Physical Society and IOP Publishing Ltd

the curve of $P(v)$ appears as a straight line after exceeding the most probable velocity, indicating that $P(v)$ approximately follows the exponential decay law in this segment. The most probable velocity is around 0.8 μm/min, which is about three times smaller than the mean velocity $v_{\rm m} = 2.4\,\mu$m/min (dotted line), which indicates that the proportion of high-speed cells is significant within the entire community.

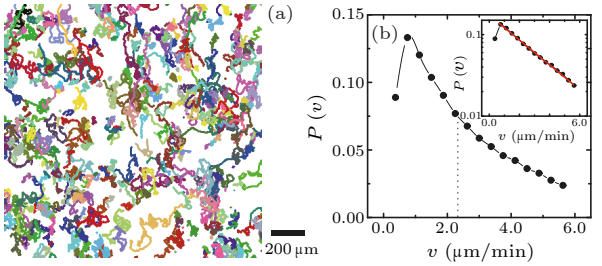

Fig. 1. (a) Trajectories of migrating Dicty cells. (b) The probability distribution of Dicty cell speed, $P(v)$. The dotted line shows the location of mean speed $v_{\rm m} = 2.3\,\mu$m/min. The inset in (b) illustrates the semi-log plot of $P(v)$, where the red solid line represents the fitting result of the equation $P(v) = k \cdot \exp(-v/v_{\rm e})$ with $v_{\rm e} = 2.9\,\mu$m/min.

We can generate a speed–acceleration phase diagram to illustrate the evolution of cell states, as shown in Fig. 2. In Fig. 2, the position of each grid point represents a cell state, denoted by the values of cell speed v and acceleration a. The arrow at each grid point indicates the trend of cell state change, with the direction representing the direction of change in the subsequent moment in the a–v phase diagram and the length of the arrow representing the rate of this trend change.

The implementation method of Fig. 2 is as follows. First, we calculate the cell speed v and acceleration a for each moment. Then, we determine the rate of change of speed and acceleration for the cells in the next moment. Here, the rate of speed change is represented by a itself, while the rate of acceleration change is defined as $b \equiv \Delta a/\Delta t$. Subsequently, we group all the velocities and accelerations obtained for all cells and all moments. Cells with similar velocities $v \in (v-\Delta v v+\Delta v)$ and accelerations $a \in (a - \Delta a a + \Delta a)$ are grouped together. Here, Δv and Δa represent half of the grouping ranges. Grouped data of (a, b) that are placed into corresponding $(a,\ v)$ grid points on the phase diagram are averaged. The average values of a and b are obtained on each $(a,\ v)$ grid point, and are represented by arrows. The direction of the arrow indicates the direction of cell movement on the phase diagram in the next moment. The shape of the arrow is clearly a function of the grid point position $(a,\ v)$, which represents the current cell state.

Figure 2 shows that the motion of the cell is centered around an attractor ($a = 0\,\mu$m/min^2, $v = 2.4\,\mu$m/min). This is a stable point characterized by the rate of change of its acceleration $b = 0\,\mu$m/min^3. In this state, the cell reaches its most stable speed, referred to as inherent speed $v_0 = 2.4\,\mu$m/min. Any deviation from this stable point will ultimately lead the cell back to this point following the direction of the streamlines in the phase diagram. In comparison of Figs. 2 and 1(b), we find that this stable velocity does not correspond to the most probable velocity, whereas it is rather closer to the mean speed $v_{\rm m}$.

One evident feature of Fig. 2 is that the further the cell deviates from the stable point, the greater the rate of change in its state (represented by longer arrows), suggesting that the cell needs to accelerate more to return to the stable point, qualitatively similar to the properties of Hooke's law. Another feature is that the rate of change in the phase diagram is not symmetric on both sides of $v = v_0$. The rate of change is greater on the side where $v < v_0$ while it is slightly slower on the side where $v > v_0$. This indicates that the cell maintains its high-speed state for longer, but tends to quickly return to a stable state at low speeds.

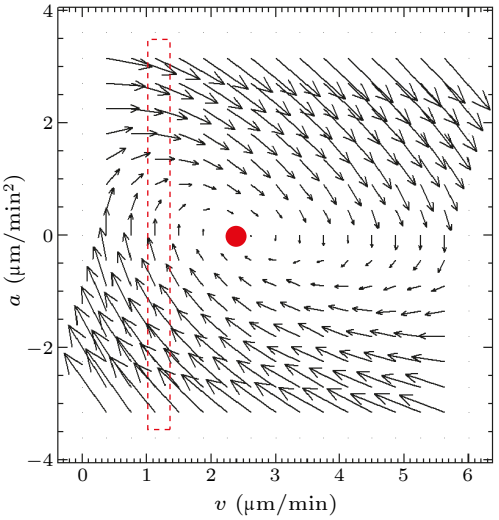

Fig. 2. Speed–acceleration (v–a) phase diagram of cell migration. The arrows represent the rates of of speed and acceleration changes at each grid point. The vertical component of the arrow represents b (rate of acceleration change) while the horizontal component represents a (rate of speed change). The red dot represents the fixed point. The vertical length of the arrows in the figure are reduced by ten times so as to clarify the location of the attractor substructure and the fixed points.

In order to further analyze the characteristic information contained in the phase diagram, we plot the trend of variation of b on the acceleration a for each speed v, as shown in Fig. 3. Specifically, in the phase diagram we take a vertical rectangular box (i.e. a given v), shown by dashed lines in Fig. 2. We use the length of the horizontal component of the arrows (a) as the horizontal axis, and use the length of the vertical component of the arrows (b) as the vertical axis.

Figure 3 shows that the plot of $b(a)$ follows a linear trend for each speed v. Additionally, the slopes of the $b(a)$ curves are similar, indicating that the rule for $b(a)$ remains the same under different speeds v. We fit the curves using

the equation

$$b = b_0 - a \cdot k_a, \tag{1}$$

where b_0 represents the intercept of the curve while k_a represents the slope. The minus sign in the equation indicates that when the acceleration is not zero, the change in cell acceleration b tends to bring the acceleration a back to zero. Moreover, the trend of recovery is linearly related to the deviation. Quantitatively, this resembles a form similar to Hooke's law, as speculated above. Each curve in Fig. 3 corresponds to a speed v. There is a clear decreasing trend in the intercept b_0 as v increases. The value of b_0 represents the rate of change of acceleration when the acceleration a is zero, here we refer to it as the inherent rate of acceleration change for the cells.

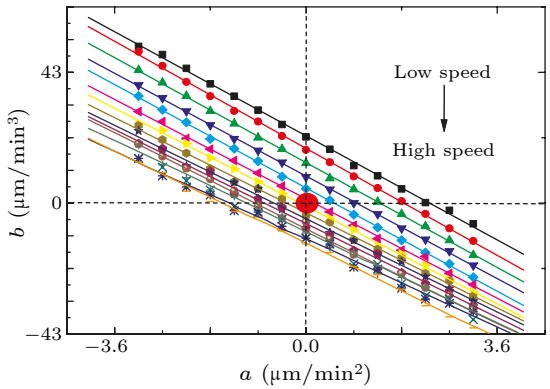

Fig. 3. Plots of the rate of change of acceleration b and acceleration a. From top to bottom, each plot corresponds to a different cell speed v, read from the horizontal axis of Fig. 2 from left to right. The straight lines in the figure represent the linear fitting results by Eq. (1). The red dot represents the stable state, corresponding to the fixed point in Fig. 2.

The dependence of b_0 and k_a on speed v is plotted in Fig. 4.

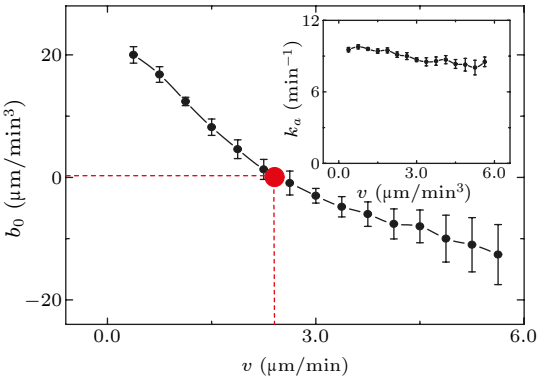

Fig. 4. Dependence of b_0 on the speed v, obtained by fitting the curves in Fig. 3 using Eq. (1). The inset illustrates the relationship between k_a and v. The red dot represents the stable state. The error bars indicate the fitting error.

Figure 4 shows that the inherent rate of acceleration change b_0 has a nonlinear negative correlation with speed v. The farther the speed v deviates from $v_0 = 2.4\,\mu\text{m/min}$ the greater the absolute value of b_0. This represents that the cells have an accelerating recovery tendency, but they slowly approach the stable point. On the side of $v < v_0$, the inherent rate of change of b_0 with respect to v is higher, for $v > v_0$ the inherent rate of change of b_0 is slower. This is consistent with the characteristics shown in Fig. 2. Thus, the asymmetrical trend in Fig. 2 is mainly contributed by the inherent rate of acceleration change for the cells, b_0.

The inset in Fig. 4 shows that, within the speed range measured, $k_a \approx 8.5 \pm 0.9\,\text{min}^{-1}$, having a slight decrease with increasing v. From the dimensional analysis of k_a we can define a characteristic time $\tau_a = 1/k_a \approx 0.12\,\text{min}$, which represents the characteristic time of the internal acceleration change of the cells. It can be seen that this characteristic time is independent of the cellular state a and is also insensitive to v.

Equation (1) indicates that, for each cell speed v, there is a specific acceleration a that can make $b = 0$. Therefore, we refer to this specific acceleration as the inherent acceleration for the cell, a_v, and its value can be obtained from $a_v(v) = b_0(v)/k_a(v)$. We plot the $a_v(v)$ curve in Fig. 5(a).

Figure 5(a) depicts that the inherent acceleration a_v has a linear relationship with cell speed v, but the slope is not the same when $v > v_0$ or $v < v_0$. We can use Eq. (2) to describe this relationship:

$$a_v = \beta \cdot (v_0 - v). \tag{2}$$

When $v < v_0$, the slope $\beta = 1.1\,\text{min}^{-1}$; when $v > v_0$, $\beta = 0.54\,\text{min}^{-1}$. Similarly, we can define the time $\tau_v = 1/\beta$ to characterize the time of cell speed change, which is τ_v =0.9 min for $v < v_0$ and τ_v =1.9 min for $v > v_0$. This means that the deceleration trend of cells on the high-speed side is about half the acceleration trend on the low-speed side.

Based on the clear physical meaning of a_v, we replace k_a in Eq. (1) with a_v, and rewrite Eq. (1), with $a_v = b_0/k_a$, as

$$b = b_0(v) \cdot \left(1 - \frac{a}{a_v(v)}\right). \tag{3}$$

From Figs. 3 and 4, we note that $a_v(v)$ and $b_0(v)$ have similar trends. We speculate that they should not be independent. Through dimensional analysis, we establish the following relationship:

$$b_0 = \gamma \cdot \frac{a_v^2}{(v_0 - v)}, \tag{4}$$

where γ is a dimensionless parameter. We verify Eq. (4) by plotting the curve of $b_0 \cdot (v_0 - v)$ versus a_v^2 using the experimental data curves in Figs. 3 and 4, and examine if the curve exhibits a linear trend. The result is shown in Fig. 5(b). Here, for clarity, we multiply the abscissa by the sign of $v_0 - v$ to avoid both lines being on the same side. The positive region of the abscissa represents the low-speed range ($v < v_0$), while the negative region represents the high-speed range ($v > v_0$). Equation (4) states that the inherent rate of change of acceleration for the cells, b_0, is proportional to the square of the inherent acceleration, a_v, and inversely proportional to the difference between

the inherent speed and the current speed $(v_0 - v)$. The fit results of Fig. 5(b) indicate that the parameter γ takes different constant values on either side of v_0. At low speeds, $\gamma = 0.85$, while at high speeds, $\gamma = 1.66$, differing by a factor of 2, in similar rules as for β in Eq. (2).

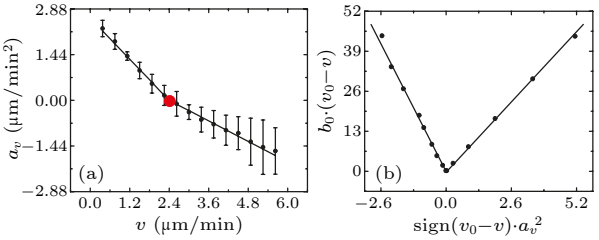

Fig. 5. (a) The relationship between the intrinsic acceleration a_v and cell speed v. The line represents the fitting results of Eq. (2). The red dot represents the stable state. (b) The verification curve of the relationship between the rate of change of intrinsic acceleration b_0 and the intrinsic acceleration a_v [according to Eq. (4)]. Sign$(v_0 - v)$ denotes the positive or negative sign. The lines are guides for the eyes.

Based on the above equations and discussions, τ_v and τ_a represent the time required for the cell's velocity and acceleration, respectively, to return to stable values. Notably, in the low-speed state, the cell's velocity recovers at a faster rate, approximately twice as fast as the recovery in the high-speed state. Moreover, τ_v remains unaltered with cell speed when in certain states, indicating non-continuous transitions between the high-speed and low-speed states but a rather distinct switch centered around v_0 as the critical point.

Considering that the characteristic time during deceleration ($\tau_v = 1.9$ min) is approximately twice as long as during acceleration ($\tau_v = 0.9$ min), it is reasonable to assume that the deceleration process is partially, if not entirely, passive. This is due to the fact that if the disassembly of the cytoskeleton is a similar active process to assembly, the characteristic time during deceleration will be comparable to or even shorter than during acceleration (as disassembly may be facilitated by thermal motion).

In sharp contrast, τ_a remains constant regardless of changes in the high-speed and low-speed states, with a minute variation of approximately 10% within the margin of error. Numerical analysis reveals that τ_a is approximately an order of magnitude smaller than τ_v, suggesting that velocity recovery and acceleration recovery may be two relatively independent physiological processes for the cell, with the latter exhibiting a significantly faster rate.

Substituting Eqs. (2) and (4) into Eq. (3), we have

$$\frac{da}{dt} = \gamma \cdot \beta^2 \cdot \left(v_0 - v - \frac{a}{\beta}\right), \tag{5}$$

$$a = \frac{dv}{dt}. \tag{6}$$

In the end, Eqs. (5) and (6) represent the dynamical model of cell motion established by our experimental measurements. By using the above values of γ, β, and v_0, we numerically calculate the speed–acceleration (v–a) phase diagram by the model of Eqs. (5) and (6). The result is shown in Fig. 6.

Comparing Figs. 2 and 6, as is expected, we can see that they are in excellent agreement. The dynamical model of Eqs. (5) and (6) can accurately describe the behavioral characteristics of cell migration. It is worth noting that in the model we treat the coefficient of speed in Eq. (5) as a constant. In the experimental data, there is a slight variation of 20% in k_a with speed (inset in Fig. 4). However, we approximately treated it as a constant in previous discussion, attributing the main features in the phase diagram to the variation in b_0 in Eq. (1). Equation (5) indicates that the stable velocity v_0 alone does not constitute the stable state of a cell; it also requires the acceleration to be zero in order to reach a dynamically stable point. Looking at the similarity between Figs. 6 and 2, we find that such an approximation is quite reasonable.

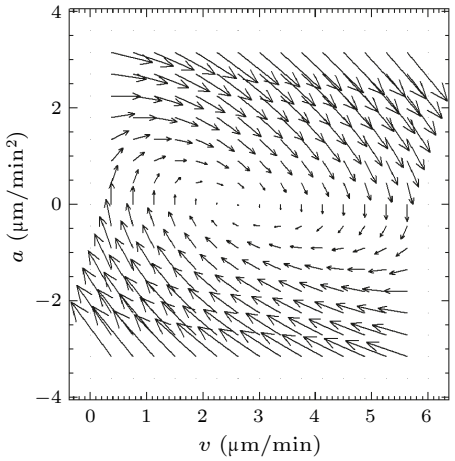

Fig. 6. The speed–acceleration (v–a) phase diagram obtained by numerically calculating the model expressed by Eqs. (5) and (6).

In summary, we have analyzed the behavioral trajectories of cell migration obtained from experiments. Using classical nonlinear dynamics methods, we plot the speed–acceleration phase diagram of Dicty cell motion. We obtain a series of characteristic parameters to describe cell migration behavior, including the inherent cell speed v_0, the characteristic time of speed change τ_v, and the characteristic time of acceleration change τ_a. Moreover, we find that the inherent rate of acceleration change b_0 is proportional to the square of the inherent acceleration a_v. Finally, through dimensional analysis and in combination with experimental data, we construct a model comprising differential equations to described Dicty cell motion, and the numerical results are well consistent with the experimental results. The parameters and values derived from the phase diagram are highly beneficial in quantitatively characterizing and classifying complex systems such as cell motion, similar to how the Reynolds number and Nusselt number help describe fluid dynamic systems.

Acknowledgment. This work was supported by the National Natural Science Foundation of China (Grant No. 31971183).

References

[1] Lauffenburger D A and Horwitz A F 1996 *Cell* **84** 359
[2] Codling E A, Plank M J, and Benhamou S 2008 *J. R. Soc. Interface* **5** 813
[3] Petrie R J, Doyle A D and Yamada K M 2009 *Nat. Rev. Mol. Cell Biol.* **10** 538
[4] Loeber J, Ziebert F, and Aranson I S 2014 *Soft Matter* **10** 1365
[5] Li L, Cox E C and Flyvbjerg H 2011 *Phys. Biol.* **8** 046006
[6] Dieterich P, Preuss R, and Schwab A 2008 *Proc. Natl. Acad. Sci. USA* **105** 459
[7] Metzler R and Klafter J 2000 *Phys. Rep.* **339** 1
[8] Roumen T and Lensen M C 2013 *Chin. Phys. Lett.* **30** 070501
[9] Czirok A, Madarasz E, and Vicsek T 1998 *Phys. Rev. Lett.* **81** 3038
[10] Liu Y P, He D, Jiao Y, Li G Q, Zheng Y, Fan Q H, Wang G, Yao J R, Chen G, and Liu L Y 2021 *Chin. Phys. B* **30** 090505
[11] Shenderov A D and Sheetz M P 1997 *Biophys. J.* **72** 2382
[12] Zhang J Z, Li N, and Chen W 2018 *Chin. Phys. B* **27** 028705
[13] Begemann I, Saha T, Lamparter L, Rathmann I, Grill D, Golbach L, Rasch C, Keller U, Trappmann B, Matis M, Klingauf J, and Galic M 2019 *Nat. Phys.* **15** 848
[14] Yooer C F, Wei F, Xu J X, and Zhang X H 2011 *Chin. Phys. Lett.* **28** 030501
[15] Brückner D B, Fink A, Schreiber C, Röttgermann P J F, Rädler J O, and Broedersz C P 2019 *Nat. Phys.* **15** 595
[16] Goldbeter A, Gonze D, Houart G, Halloy J, and Dupont G 2001 *Chaos* **11** 247
[17] Levine H, Tsimring L, and Truong T V 1996 *Proc. Natl. Acad. Sci. USA* **93** 6382
[18] Shams D P, Mehta P, and Schwab D J 2020 *Phys. Rev. E* **101** 062410
[19] Chen S, Li N, Hsu S F, Zhang J, Chan C K, and Chen W 2014 *Soft Matter* **10** 3421